Modelling and Simulation in Materials Science and Engineering

PAPER

Density functional theory investigations of titanium γ-surfaces and stacking faults

To cite this article: Magali Benoit *et al* 2013 *Modelling Simul. Mater. Sci. Eng.* **21** 015009

Modelling Simul. Mater. Sci. Eng. **21** (2013) 015009 (17pp) doi:10.1088/0965-0393/21/1/015009

Density functional theory investigations of titanium γ-surfaces and stacking faults

Magali Benoit[1], **Nathalie Tarrat**[1] **and Joseph Morillo**[1,2]

[1] CEMES-CNRS UPR 8011, 29 rue Jeanne Marvig, 31055 Toulouse Cedex, France
[2] Université Paul Sabatier, 118 route de Narbonne, F-31062 Toulouse Cedex 9, France

Received 29 February 2012, in final form 28 September 2012
Published 19 December 2012
Online at stacks.iop.org/MSMSE/21/015009

Abstract

Bulk properties of hcp-Ti, relevant for the description of dislocations, such as elastic constants, stacking faults and γ-surface, are computed using density functional theory (DFT) and two central force embedded atom interaction models (Zope and Mishin 2003 *Phys. Rev.* B **68** 024102, Hammerschmidt *et al* 2005 *Phys. Rev.* B **71** 205409). The results are compared with previously published calculations, except pair potential calculations, which are not appropriate for the description of the metallic bond. The comparison includes N-body central force (NB-CF) and N-body angular (NB-A) empirical potentials, tight-binding approximation to the electronic structure (TB), DFT pseudopotential (DFT-P) and all electron (DFT-A) calculations. None of the considered interaction models are fully satisfactory for the description of these properties. In particular, NB-CF, NB-A and TB interaction models are unable to describe the softening of the easy prismatic γ-surface leading to the appearance of a metastable stacking fault, as evidenced in all the DFT calculations. Most often, when the basal stacking fault excess energy is underevaluated, this leads to an inversion of the energetic stability between the I_2 basal and the prismatic easy stacking faults. Even the DFT-pseudopotential calculations need to be improved regarding the description of the shear elastic constants. The implications of these results on the core structure and gliding properties of the $a/3\,\langle 11\bar{2}0\rangle$ screw dislocation are analyzed. The calculated dissociation lengths into Shockley partials in both the basal and prismatic planes for the different models compare well with the measured ones in the corresponding simulations of the dislocation core structure when available. Finally, the Peierls stress is also evaluated using the Peierls–Nabarro model and compared with the experimentally measured one.

(Some figures may appear in colour only in the online journal)

1. Introduction

The plastic behavior of hexagonal compact metals (about 20) is dominated by the movement of dislocations with the shortest Burgers vector: $\frac{a}{3}\langle 1\,1\,\bar{2}\,0\rangle$ (see [3, 4] for recent reviews). For example, most of the transition metals have a basal slip plane, but three of them (Zr, Ti and Hf) and a number of rare-earth metals (Gd, Ru, Tb, Hf, Dy and Er) present a dominant prismatic slip plane [4–7]. The intrinsic characteristics of dislocations (structure, stability, mobility, formation, multiplication) as well as their extrinsic characteristics (interaction with impurities, point defects, grain boundaries etc) are therefore essential ingredients for a good theoretical description of the plastic behavior of hexagonal compact (hcp) metals.

The core structure of the $\frac{a}{3}\langle 1\,1\,\bar{2}\,0\rangle$ screw dislocation in hcp metals has been subjected to only a few theoretical studies (see [6] for a recent review). Legrand, who introduced an explicit treatment of the electronic degrees of freedom in a tight-binding (TB) approach [7, 8], was the first one to obtain a prismatic spreading in an hcp metal (Ti). Moreover, this prismatic spreading was energetically more favorable than the basal one by 24 meV Å^{-1}. He argued that this prismatic preference was related to an increased basal stacking fault energy of transition metals with d fillings between 1.5 and 2.5 electrons. This effect results from the directional d-covalent bonding of partially filled d bands, which cannot be described with pair potentials or with more sophisticated central force N-body potentials. More precisely, he established [7, 9, 10], on the basis of his TB calculations (and pseudopotential calculations for divalent and trivalent metals), a clear correlation between the basal or prismatic slip in hcp metals and the ratio $R = (\gamma_b/C_{44})/(\gamma_p/C_{66})$. γ_b and γ_p are, respectively, the basal I_2 and the prismatic stacking fault excess energies and C_{44} and C_{66} are the shear elastic constants governing the shear deformation leading to the corresponding stacking fault. This ratio measures the relative facility to form both stacking faults and thus the easiness of dislocation dissociation in the corresponding planes. For $R > 1$, the observed slip should be prismatic, whereas it should be basal for $R < 1$. One must note that, in all his calculations, he never found a stable prismatic stacking fault, but the γ_p-surface presented a deep valley in the $\langle\bar{1}\,2\,\bar{1}\,0\rangle$ direction. He then defined the stacking fault excess energy as an average value of the γ_p surface energy in this direction, corresponding to a continuous dislocation spreading. Notwithstanding, in principle, their inability to describe the directional character of the bonding in Ti, pair potentials and N-body central force potentials have been able to reproduce the preferential prismatic core structure of the $\frac{a}{3}\langle 1\,1\,\bar{2}\,0\rangle$ screw dislocation in some cases [11, 12].

More recently, Girshick and co-workers [13] derived a bond order (BO) potential for Ti [14] allowing them to deduce more accurate values of the excess energies of the basal and prismatic dislocation cores. With the BO potential, in agreement with Legrand [7, 8], they found that the prismatic core was the most stable one (by about 20 meV Å^{-1} relative to the basal one). At odds with the BO potential, the N-body Finnis–Sinclair central force potential [15], which they used for comparison, favored the basal spreading (by about 25 meV Å^{-1}). In agreement with Legrand, they did not find any stable prismatic stacking fault. Most importantly, from their BO calculations, they obtained a $R = 0.4$ value, which means a preferential basal spreading in contradiction with their determination of the core structure energies, which questions the validity of Legrand's criterion.

However, prior to our preliminary study [16], there was only one density functional theory (DFT) calculation of the $\frac{a}{3}\langle 1\,1\,\bar{2}\,0\rangle$ screw dislocation in hcp metals (Zr and Ti) [17, 18]. In this work, an unique prismatic spreading with a core structure in overall agreement with the previous TB calculations [7, 8, 13] was obtained. In [16], we identified a possible metastable structure, a result which was later confirmed in another DFT calculation, using different boundary conditions, pseudopotential and basis set [19].

The purpose of this paper is to give a comprehensive review of the present theoretical knowledge of the bulk properties, stacking faults and γ-surfaces, which are essential properties to gain a deeper understanding of the relationship between the electronic structure of hcp Ti and its plastic behavior. Previously published calculations, except for pair potential calculations, which are not appropriate for the description of a metallic bond, will be compared with our own DFT calculations and embedded atom model (EAM) calculations performed with recently developed accurate semi-empirical EAM potentials [1, 2]. These two EAM potentials were specifically designed to reproduce a large database of properties in TiAl [1] or Ti [2], either experimentally measured or deduced from *ab initio* DFT calculations. This database includes a large panel of configurations far from the ideal hcp lattice, so these potentials might be accurate for the description of the dislocation core structure. The comparison will include, from the least precise class of calculation to the most accurate one, N-body central force (NB-CF) and N-body angular (NB-A) empirical potentials, tight-binding approximation to the electronic structure (TB), DFT pseudopotential (DFT-P) and all electron (DFT-A) calculations, which are ordered in each class from the oldest to the most recent ones.

After giving the simulation details of our calculations in section 2, we present in section 3 the comparative study of the hcp Ti properties, bulk properties in section 3.1, stacking faults in section 3.2 and γ-surfaces in section 3.3. These results are then discussed with particular focus on their implications on the plastic behavior of hcp Ti in section 4.

2. Simulation details

2.1. DFT calculations

DFT calculations were performed with the SIESTA [20] code in which the orbitals are developed on a local basis set. The PBE-GGA gradient approximation [21] was used for the exchange and correlation functional and the pseudopotential was a Trouiller–Martins [22] one, with the 3p4s3d states as valence states. A polarized double-ζ basis set was employed for the 4s electrons and a single-ζ basis set was employed for the 3p and 4d electrons. The choice of the functional, basis sets and pseudopotentials was made in order to reproduce experimental structural characteristics. Moreover, the use of a localized basis set will allow us to perform calculations on screw dislocations in the cluster approach at a lower computational cost than with a plane-wave basis set.

A 500 Ry real space grid cutoff and a Methfessel–Paxton smearing of order one with an electronic temperature of 300 meV were used in all calculations. For the bulk calculations, performed with the conventional primitive cell, a $11\times11\times7$ k-point mesh was used for the first Brillouin zone sampling, which was extended to a $16\times16\times12$ mesh for the determination of some of the elastic constants. For the other calculations, the specific k-point mesh will be given in the corresponding section. In all calculations, the structural relaxations were carried out until the force differences were less than 5 meV Å^{-1}.

2.2. Semiempirical potential calculations

The two semiempirical potentials are of the embedded atom method [23] type. The first one (referred to hereafter as ZM) was developed by Zope and Mishin [1] for the TiAl alloy. They fitted their Ti potential to experimental data (lattice parameters: a, c/a, cohesive energy E_c and the five independent elastic constants C_{ij}) and to the *ab initio* DFT volume–pressure curves of various crystal structures (hcp, face-centered cubic (fcc), body-centered cubic (bcc), simple cubic (sc) and ω). Our calculations were performed using the tabulated functions of the ZM

potential, retrieved from their website, and cubic splines in between the tabulated points. Thus, due probably to the use of a different spline algorithm, our ZM potential is not exactly the same as the original one, leading to slightly different elastic constants, but without any significant differences in the basal stacking fault energies. Its cutoff distance is in between the fourth and fifth neighbor shells. The second one (referred to hereafter as HKV) was developed by Hammerschmidt and co-workers [2] for the description of grain boundaries. It was also fitted to bulk Ti properties and to a large database of low coordinated configurations, namely small clusters (up to eight atoms), surfaces and adatom surface diffusion. Its cutoff distance is in between the third and fourth neighbor shells. Both of them are then expected to be able to describe configurations far from the ideal hcp structure.

In all calculations, where periodic conditions were applied in a given direction, the simulation cell dimension in that direction was set to at least five times the interaction cutoff in order to avoid any spurious interaction of an atom with its periodic images.

3. Results

3.1. Bulk properties

In tables 1 and 2, the bulk properties of hcp Ti of interest for the description of dislocations in pure Ti, calculated with GGA-DFT and the two EAM potentials, are compared with previous calculations and with experimental data. In both tables, values, unless otherwise stated (300 K), are $T = 0$ K values. Table 1 reports the parameters describing the hcp Ti lattice under equilibrium conditions, lattice constants and the corresponding cell volume, and its response to an isotropic stress, the bulk modulus. The responses of the hcp Ti lattice to a general stress tensor, i.e. the elastic constants, are given in table 2 together with the two Cauchy pressures, which measure the ability of the model to reproduce N-body effects. To the best of our knowledge, these tables report a comprehensive list of all the previously published calculations, except for the first published EAM potential [24], which lead to c/a ratios very close to the ideal ratio and very low stacking fault energies [25], and for the pair potentials calculation, which is not appropriate for the description of the metallic bond. This includes, from the least precise class of calculation to the most accurate one, N-body central force (NB-CF) and N-body angular (NB-A) empirical potentials, tight-binding approximation to the electronic structure (TB), DFT pseudopotential (DFT-P) and all electron (DFT-A) calculations, which are ordered in each class from the oldest to the most recent ones. We only retained those calculations that gave at least the bulk modulus or stacking fault energies (see table 3). For the DFT calculations, we retained only those performed within the GGA exchange-correlation functional, since it is known to best reproduce the bulk properties than the LDA one.

All models reproduce the deviation from the ideal c/a ratio and the bulk modulus with comparable accuracy. Compared with other DFT calculations, the DFT SIESTA pseudopotential calculations (the present one and the one of [39]) tend to overestimate the cell volume while keeping the right c/a ratio. More pronounced deviations occur in the TB scheme calculations when they are performed at the experimental instead of the model equilibrium volume [34, 35]. An unexpected larger bulk modulus is also observed in the DFT-A calculation of [43] at $T = 300$ K, whereas the bulk modulus decreases slightly with temperature. However, since we deduced this value from their $V(P, T = 300\,\text{K})$ curve, it is not very precise.

For the elastic constants (table 2), the agreement between the DFT calculations and experiment is satisfactory (deviations less than 10%). The differences between the calculations can be due to the use of different exchange-correlation functionals and basis sets, convergence

Table 1. Hcp Ti lattice parameters a (Å) and c/a, corresponding primitive cell volume V_0 (Å^3) and bulk modulus B (GPa). Comparison of the present results (the two EAM potentials and the DFT calculations) with the experimental data and with the previously published ones: N-body central force (NB-CF) and N-body angular (NB-A) empirical potentials, tight-binding approximation to the electronic structure (TB), DFT-GGA pseudopotential (DFT-P) and all electron (DFT-A) calculations.

Model	a	c/a	V_0	B	Ref.
NB-CF	2.951	1.588	17.67	109.97[a]	[25]
	2.951	1.592	17.71	117.6	[15]
	2.942	1.587	17.50	106.6	[26]
	2.951	1.585	17.64	111.4 (110.5)	ZM [1] This work
	2.969	1.590	18.02	110.4	HKV This work
	2.950	1.586	17.64	114.1	[27]
NB-A	2.951	1.588	17.67	110.0	[28]
	2.951	1.584	17.63	105.1	[29]
	2.951	1.588	17.67	110.0	[30] from [1]
	2.9506	1.586	17.64	105	[31]
	2.945	1.592	17.60	109.7	[32]
	2.931	1.596	17.40	112.7	[33]
TB	2.97	1.616	18.33	122 (93.9)[b]	[34]
	2.950	1.587	17.64	113.8	[14]
	2.943	1.548	17.08	(91)[b]	[35]
	2.94	1.602	17.63	109	[36]
DFT-P	2.94	1.589	17.49	—	[18, 37]
	2.93	1.589	17.31	112.5[a]	[38]
	2.95	1.586	17.64	110.9	[36]
	2.99 (2.93)	1.588 (1.581)	18.38 (17.22)	107 (115)	[39][c]
	2.947	1.583	17.55	110.9	[33]
	2.94	1.58	17.39	—	[40]
	2.996	1.588	18.49	110.2	This work
DFT-A	2.934	1.588	17.36	114	[41]
	2.942	1.589	17.53	113	[42]
	2.95	1.580	17.6	133	[43][d]
	2.952	1.588	17.69	—	[36]
Exp.	2.951	1.585	17.64	—	[44]
	—	—	—	110	$T = 4$ K [45, 46, 47]
	—	—	—	107	$T = 298$ K [45, 46, 47]

[a] Frozen internal degrees of freedom.
[b] In parentheses as deduced from the C_{ij} calculated at the experimental volume (table 2).
[c] SIESTA calculations, in parenthesis VASP calculations.
[d] 300 K values extracted from their $V(P, T = 300\,\text{K})$ curve.

criteria and rounding errors. Since there have not been any all electron calculations of the elastic constants, it is not possible to attribute the deviations from the experimental results to the pseudopotential or to the exchange-correlation functional approximation, notwithstanding the experimental uncertainties. Concerning the other approaches, one must consider first that, in some calculations, by construction, the elastic constants are exactly reproduced. This is the case for one BN-CF potential (EAM of [25]) and one NB-A potential (modified embedded atom model, MEAM, of [28]). We did not observe a systematic improvement when going from NB-CF, to NB-A up to TB class of calculations, despite the fact that one expects an increasingly better reproduction of N-body effects. The agreement is poorer than with DFT

Table 2. Hcp Ti elastic constants C_{ij}, and Cauchy pressures $CP_1 = C_{12}$–C_{66} and $CP_2 = C_{13}$–C_{44} in GPa. Comparison of the present results (the two EAM potentials and the DFT calculations) with the experimental data and with the previously published ones: N-body central force (NB-CF) and N-body angular (NB-A) empirical potentials, tight-binding approximation to the electronic structure (TB) and DFT-GGA pseudopotential (DFT-P).

Model	C_{11}	C_{12}	C_{13}	C_{33}	C_{44}	C_{66}	CP_1	CP_2	Ref.
NB-CF	176.1	86.9	68.3	190.5	50.8	45.1	41.8	17.5	[25][a]
	180.0	87.4	76.6	217.0	51.4	46.4	40.9	25.2	[15]
	147.3	78.5	76.4	198.0	30.5	34.4	44.1	45.9	[26]
	178	74	77	191	51	52	22	26	ZM [1]
	186.2	69.5	76.2	189.4	46.4	58.3	11.2	29.8	ZM This work
	188.6	65.4	67.4	216.9	45.8	61.6	3.8	21.6	HKV This work
	131.2	59.3	94.0	270.0	70.5	36.0	23.3	23.5	[27]
NB-A	176.1	86.9	68.3	190.5	50.8	44.6	42.3	17.5	[28]
	177.8	77.9	64.7	175.6	46.8	50	27.9	17.9	[29]
	189	74	68	188	50	57.5	16.5	18.0	[30] from [1]
	160	90	66	181	46.5	35	55	19.5	[31][a]
	170.1	80.4	74.8	187.1	42.1	44.9	35.6	32.7	[32]
	174	95	72	188	58	39.5	55.5	14	[33]
TB	171	58	46	203	64	56.5	1.5	−18	[34][b]
	176.1	74.0	83.3	190.5	50.8	51.1	22.9	32.5	[14]
	127	81	64	147	45	23	58	19	[35][b]
	155	91	79	173	65	32	59	14	[36]
DFT-P	—	—	—	—	43	45	—	—	[18, 37]
	171.6	85	78.6	187.5	39	43.3	41.7	39.6	[38][a]
	172	82	75	190	45	45	37	30	[36, 33]
	162(181)	94(83)	69(79)	175(191)	33(44)	34(49)	60(34)	36(35)	[39][c]
	183.4	84.6	63.8	204.9	48.8	49.4	35.2	15.0	This work
Exp.	176.1	86.9	68.3	190.5	50.8	44.6	42.3	17.5	$T = 4$ K [45, 46, 47]
	162.4	92	69	180.7	46.7	35.2	56.8	22.3	$T = 298$ K [45, 46, 47]

[a] Frozen internal degrees of freedom.
[b] Calculated at the experimental volume and for the c/a that minimizes the energy.
[c] SIESTA calculations, in parentheses VASP calculations.

calculations, with very large deviations in the NB-CF calculation of [27]. Nevertheless, there are no significant deviations from the experimental values (less than 15% in general), except for the shear constants C_{44} and/or C_{66} for which deviations up to 40% are observed in some cases. In the NB-CF calculations of [1, 26, 27], in our HKV calculation, and for the NB-A calculations of [30, 32], there is even an inversion of the strength between C_{66} and C_{44}. This is also the case for the TB-type BO calculation of [14]. Clearly, the interaction models have some difficulty in reproducing these shear constants properly, leading to an erroneous anisotropy ratio C_{44}/C_{66}. From this point of view, most of the NB-CF models seem to be more accurate than the TB models. As a consequence, the N-body effects, measured by the Cauchy pressures, are not very well reproduced with very high deviations in some cases (the TB model of [34]). The best model seems to be the very recently published NB-A MEAM [33].

3.2. Stacking faults

Table 3 presents the calculated (present and previously published calculations) excess energies of the two intrinsic I_1 (ABAB|CBCB) and I_2 (ABAB|CACA), and the extrinsic I_E (ABAB|C|ABAB) elementary stacking faults in the basal plane, the easy prismatic $F_1 = \vec{b}/2$

stacking fault excess energy corresponding to either a true metastable stacking fault or a saddle point, and the available experimental estimations of these quantities. In our calculations we used a slab geometry with free surfaces in order to avoid any problem with a possible unsymmetric configuration of the two generalized stacking faults, necessarily present in a periodic cell calculation [40, 48, 49]. An open planar defect was also considered in order to test the different models toward low coordinated planar configurations. The (0 0 0 1) surface was chosen since it is the lowest surface energy and the most commonly calculated one. We used, in our (0 0 0 1) surface calculations, the same slab geometry as in the basal stacking fault calculation. Its excess energy was calculated in the usual way [50].

The excess fault energy γ is given by

$$\gamma = E_{\text{faulted}} - E_{\text{perfect}}, \tag{1}$$

where E_{faulted} is the total energy of the slab containing the fault, and E_{perfect} is the total energy of the perfect slab. For the DFT calculations, the size of the vacuum (4 interatomic distances, i.e. ≈9.5 Å) and the number of planes (14 atomic planes for I_1 and I_2 and 15 atomic planes for I_E) have been adjusted to have good converged results. The slabs were then relaxed, using a mesh of 12 × 12 × 2 k-points. In the EAM simulations, the slabs were made of 40 atomic planes and were replicated 8 times in the fault plane, so that the dimensions of the supercell were about 5 times the cutoff radius of the potential.

In the case of the prismatic stacking, contrary to the basal case, there is no evidence that there exist metastable easy stacking faults (see section 3.3). In fact, prior to the first DFT calculations [17, 18, 37], the existence of a prismatic easy stacking fault was controversial. Such a stacking fault was obtained only with two NB-CF EAM interaction potentials [12, 13] close to the $F_1 = \vec{b}/2$ point (see table 3), whereas *a priori* more precise calculations in the TB scheme [7, 9, 14] found only a saddle point. Possible positions, like F_1, can be inferred from symmetry considerations (intersection of symmetry planes [25, 51]). However, since the local configuration is highly perturbed for this stacking, it is not possible, as for the basal stacking, to infer that it will correspond to a local minimum prior to any calculation.

All the DFT calculations, with free surfaces or periodic boundary conditions, give very similar results, except those of [17, 18, 37] for the prismatic stacking fault value which they found 50% lower. This difference comes from the strong dependence of the excess energy with the number of planes in a slab calculation with free surfaces. In fact, in figure 1, the evolution of the prismatic stacking fault excess energy as a function of the number of atomic planes included in the calculation is presented. The excess energy starts to converge when the number of planes is at least greater than 16, but with still noticeable oscillations with the number of planes.

These oscillations are known to be due to quantum size effects, which appear for specific slab geometries leading to long-range interlayer oscillating relaxations [57–61] and consequently make the DFT calculations very sensitive to the number of planes. The present DFT value reported in table 3 is the mean value for calculations with a number of planes larger than 16. Considering the very indirect experimental determination of the stacking fault excess energies, the DFT results are satisfactory.

Contrary to what happened with the elastic constants, there are large differences between the different classes of interaction potentials in their determination of the basal I_2 stacking fault excess energy and the F_1 prismatic excess energy corresponding to the observed stacking fault in the DFT calculations. NB-CF models are not able to give the correct hierarchy between the prismatic F_1 excess energy and the basal I_2 stacking fault excess energy. They usually underestimate all the basal faults and overestimate the prismatic F_1 excess energy, leading to an inversion of the relative stability between the I_2 basal and the prismatic F_1, faults which

Table 3. Hcp Ti (0 0 0 1) surface energy γ_s and stacking fault excess energies (mJ m^{-2}): γ_{I_1}, γ_{I_2}, γ_{I_E} (0 0 0 1) stacking faults and γ_p prismatic stacking fault at $F_1 = \frac{1}{2}\vec{b}$. The Legrand's R ratio is also presented when its calculation was possible. Comparison of the present results (the two EAM potentials and the DFT calculations) with the experimental data and previously published calculations: N-body central force (NB-CF) and N-body angular (NB-A) empirical potentials, tight-binding approximation to the electronic structure (TB) and DFT-GGA pseudopotential (DFT-P); (ur): unrelaxed.

Model	γ_s	γ_{I_1}	γ_{I_2}	γ_{I_E}	$\gamma_{p,easy}$	R	Ref.
NB-CF	—	—	116	—	400 (≈400)[a]	0.26	[25, 12]
	993	33	64	94	253(350)[b]	0.23(0.17)[b]	[15, 14]
	1725	31	56	82	—		ZM [1]
	1263	30.6	54.3	82.4	341.9(364.6)[c]	0.20(0.19)[c]	ZM, This work and [16]
	1185	—	—	—	—		HKV [2]
	1188	33.6	64.5	94.2	258.5(353.6)[d]	0.34(0.24)[d]	HKV This work
	1442	68	101	200	—		[27]
NB-A	—	—	104	—	—		[28]
	1962(ur)		144(ur)		—		[29]
	1439	31	57	84	—		[30] from [1]
	1033	24	47	71	—		[31]
	2144	—	213	—			[32]
	1474	—	170-172	—	297[e]	0.39	[33, 19]
TB	—	—	290(370)	—	110(140)	2.5	[7–9][f]
	—	—	110	—	260(350)[g]	0.43(0.32)[g]	[13]
	—	44	118	—	—		[52]
DFT-P	—	—	291	—	174	1.8	[18, 37]
	1939	—	320	—	—		[33]
	1991	—	287	—	—		[40]
	—	—	292	—	220	1.3	[19, 36]
	2048	148.6(150)	259.1(260)	353.1(365)	250.0(233)	1.0(1.1)	This work and [16]
Exp.	2100	—	—	—	—		[53]
	1920	—	—	—	—		[54]
	—	—	>300	—	—		[55]
	—	—	—	—	150	1.756 ($T = 4$ K)	[56]

[a] Minimum at $\frac{1}{2}\vec{b} + 0.125\,\vec{c}$, in parantheses saddle point at F_1.
[b] Minimum at $\frac{1}{2}\vec{b} + 0.18\,\vec{c}$, in parantheses saddle point at F_1.
[c] Minimum at $\frac{1}{2}\vec{b} + 0.1\,\vec{c}$, in parantheses saddle point at F_1.
[d] Minimum at $\frac{1}{2}\vec{b} + 0.15\,\vec{c}$, in parantheses saddle point at F_1.
[e] saddle point at $\frac{1}{2}\vec{b}$.
[f] Transfer integrals to second, in parentheses to first, neighbors; $\frac{1}{2}[\gamma(0.2\vec{b}) + \gamma(0.3\vec{b})]$ for the prismatic fault.
[g] $\frac{1}{2}[\gamma(0.2\vec{b}) + \gamma(0.3\vec{b})]$ for the prismatic fault, in parenthesis saddle point at F_1.

are of interest for the analysis of dislocation slip mechanisms. This is, in particular, the case for the two EAM potentials we used despite the fact that they were chosen because they were developed in order to reproduce defects with high angular variations in titanium. It is worth noting that all the NB-CF models found a very shallow metastable prismatic fault close to the F_1 point. Concerning the NB-A models, there has been only one calculation [19, 33] of both the prismatic F_1 and the I_2 basal stacking faults, which still gives the wrong energetic ordering between these two faults. It is worth noting that in their calculations F_1 is a saddle point. The tendencies are the same as for the NB-CF models, however, the discrepancies are less pronounced. In the TB scheme, there is no clear tendency: in all calculations F_1 is a saddle

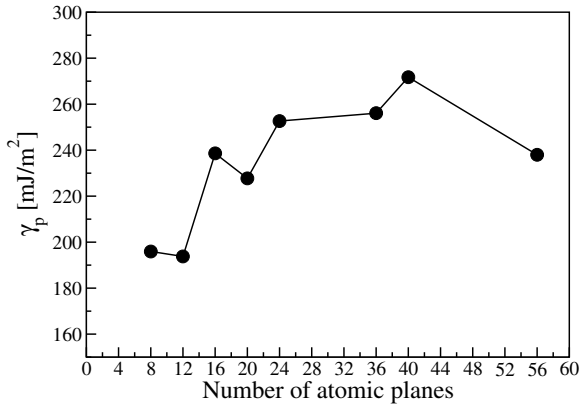

Figure 1. Evolution of the DFT prismatic stacking fault excess energy as a function of the number of atomic planes.

point, but in the original work of Legrand *et al* [7–9] the basal stacking fault excess energy is close to the DFT ones and the prismatic one is underestimated, whereas the BO potential of Girshick *et al* [13] does the reverse leading to an inversion of stability like with the NB-CF potentials. A similar underestimation of the basal fault has also been obtained in [52]. Thus, surprisingly, some of those TB results [7–9] reproduce the basal stacking fault properly and the prismatic one poorly, referring to the DFT results, whereas others [13, 52] do the reverse.

3.3. γ-surfaces

Prior to our DFT and EAM calculations, there were some determinations of the γ-surfaces in hcp Ti with NB-CF [12, 13], Nb-A [19] potentials (easy prismatic), TB approximation [9, 7, 13] and DFT-P [17, 19] (easy prismatic). In the present calculations, systems similar to the stacking faults were used, i.e. slabs with free surfaces of 14 atomic planes for the basal surface and of 15 atomic planes for the prismatic one. In the EAM simulations, the slabs were made of 40 planes of 64 atoms in the basal case and of 40 planes of 70 atoms in the prismatic case, leading to systems of 2560 and 2800 atoms, respectively. The slabs were cut into two parts, which were then shifted with respect to each other by steps of $0.005 \times a$ in the empirical simulations and of $0.01 \times a$ in the DFT ones. The atoms were allowed to relax only in the direction perpendicular to the slab surface.

The present EAM and DFT calculations give results in agreement with the previously published ones. Whatever the type of calculation, NB-CF, NB-A, TB or DFT, the general shape of the γ-surfaces are the same for a given type of γ-surface. This is clearly visible in figure 2, which presents the basal and prismatic γ-surfaces obtained with the two EAM potentials and the DFT calculation. The main differences are in the more or less pronounced extrema of the surfaces and the possible existence of local minimum at F_1 in the easy prismatic γ-surface corresponding to a metastable stacking fault. These differences can lead to a different ordering of the excess stacking fault energies between the I_2 basal and the F_1 prismatic stacking faults, as discussed in section 3.2. More precisely, the basal γ-surfaces obtained with NB-CF potentials present deep basins, which are almost nonexistent using DFT, leading to a large underestimation of the basal I_2 stacking fault with NB-CF empirical potentials. Concerning the prismatic γ-surfaces, they give lower maxima and deeper minima than the DFT ones without any local minimum at F_1 leading to an overestimation of the F_1 prismatic stacking fault.

Another striking difference between all model potentials and the DFT results is their inability to find the rather strong flattening of the prismatic γ-surface around F_1 in the $\vec{b} = \frac{a}{3}\langle 1\,1\,\bar{2}\,0\rangle$ Burgers vector direction and the associated shallow local minimum at F_1: they all found a saddle point with a much higher excess energy and, in some cases, a very shallow minimum close to F_1 in the $\vec{c}$ direction (between $0.1\vec{c}$ and $0.2\vec{c}$ depending on the model, figure 2, right). This is more visible in figure 3, where the basal and prismatic γ-lines along the Burgers vector are depicted. In the basal case (figure 3(*a*)), the differences between the DFT line and the EAM potential ones are negligible. In contrast, in the prismatic case in DFT, there is a strong flattening between $0.25\vec{b}$ and $0.75\vec{b}$ with a shallow local minimum at F_1, $\simeq 18.6\,\mathrm{mJ\,m^{-2}}$ below the maximum of the line, which is not present in the EAM cases, which leads to a much lower excess energy at F_1. This local minimum at F_1 in the DFT case indicates the existence of a stable stacking fault in the prismatic plane, and thus a possible dissociation into partial dislocations.

A similar minimum has also been evidenced in hcp Zr [17, 18]. The NB-A MEAM calculation [19] differs from the NB-CF calculations in that, instead of a minimum close to F_1, it gives a saddle point, the surface being very flat around it. It is worth noting that they also found a shallow local minimum at $\frac{1}{2}[0\,0\,0\,1]$ which has never been observed in any DFT calculation. Concerning the TB-based calculations, big differences are observed between the early TB calculations of Legrand [7–9] and the most recent BO potential of Girshick *et al* [13], leading to very different stacking fault energies, as discussed in section 3.2. In particular, Legrand's calculations lead to an R ratio larger than 1 like in the DFT case, whereas it is much lower than 1 in Girshick *et al* calculations ($R \approx 0.4$).

4. Discussion and conclusion

A detailed review of the present theoretical knowledge of hcp-Ti properties relevant for the description of dislocations, i.e. elastic constants, stacking faults energies and γ-surfaces, is presented. Concerning the elastic constants, as discussed in section 3.1, interaction models, which have not been designed to reproduce the elastic constant exactly, have in general some difficulty properly reproducing the shear elastic constants, C_{44} and C_{66}, leading to a poor description of N-body effects as evidenced by the observed bad reproduction of the Cauchy pressures CP_1 and CP_2. The only exception is the most recently published NB-A MEAM model [33], whose results are even better than some DFT calculations in particular for CP_2. Even the DFT calculations are not so good: CP_1 is rather well reproduced, whereas CP_2 is twice the experimental value except in the present SIESTA calculations. Concerning the stacking faults and the γ-surfaces, the interaction models also have difficulty describing them properly. In particular, with the exception of the pioneering TB work of Legrand [7–9], they are unable to reproduce the softening of the prismatic γ-surface around the F_1 point leading to an inversion of stability between the I_2 basal stacking fault and the excess prismatic energy at F_1, as observed in all DFT calculations. It is worth noting that, until now, fine details of the prismatic γ-surface evidenced by all the DFT calculations, such as the metastable prismatic stacking fault at F_1, could not be reproduced by any interaction model, all of them giving instead a saddle point at F_1. This is also the case for the best interaction model for the elastic constants, the NB-A MEAM model [33]. Its description of the γ-surfaces is not really satisfactory. In particular, it leads to a very low R ratio, 0.389, compared with the DFT ones which are larger than 1. As discussed in section 3.2, this is due to a strong underestimation of the I_2 basal stacking fault and an overestimation of the prismatic F_1 excess energy. This inability of the interaction models (even the TB models, which explicitly describe the valence electronic degrees of freedom in an approximated way) to reproduce important details of the prismatic γ-surface, such as its

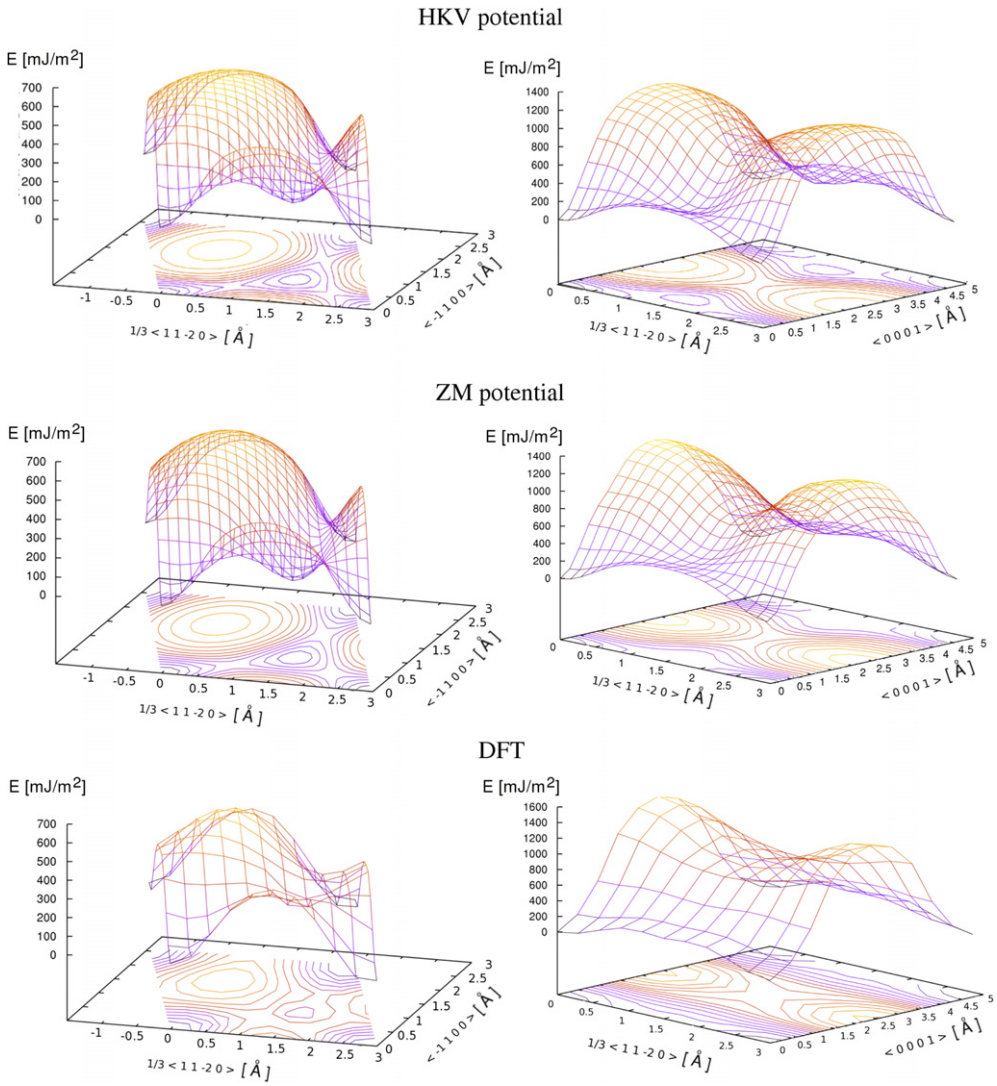

Figure 2. Hcp Ti gamma surfaces. Left: basal plane, right: prismatic plane. Top and middle: HKV and ZM EAM potential calculations, respectively; bottom: DFT calculations.

local minimum at F_1, could be problematic. In fact, it certainly means that this minimum results from subtle electronic structure effects, which will then be difficult to reproduce in any approximated description. Since the dislocation core structure and the γ-surfaces are closely related, similar effects can be expected in the description of dislocation properties that can then be difficult to reproduce with interaction models. In the same way, it appears that none of the interaction models are able to reproduce both stacking fault energies properly. In particular, the basal I_2 stacking fault energy is most often underestimated.

To conclude, none of the discussed interaction models can reproduce, with a high degree of accuracy, all the elementary properties that are closely related to the dislocations. DFT-pseudopotential calculations obviously give better results without being completely satisfactory, in particular for the shear elastic constants, and they present a large dispersion.

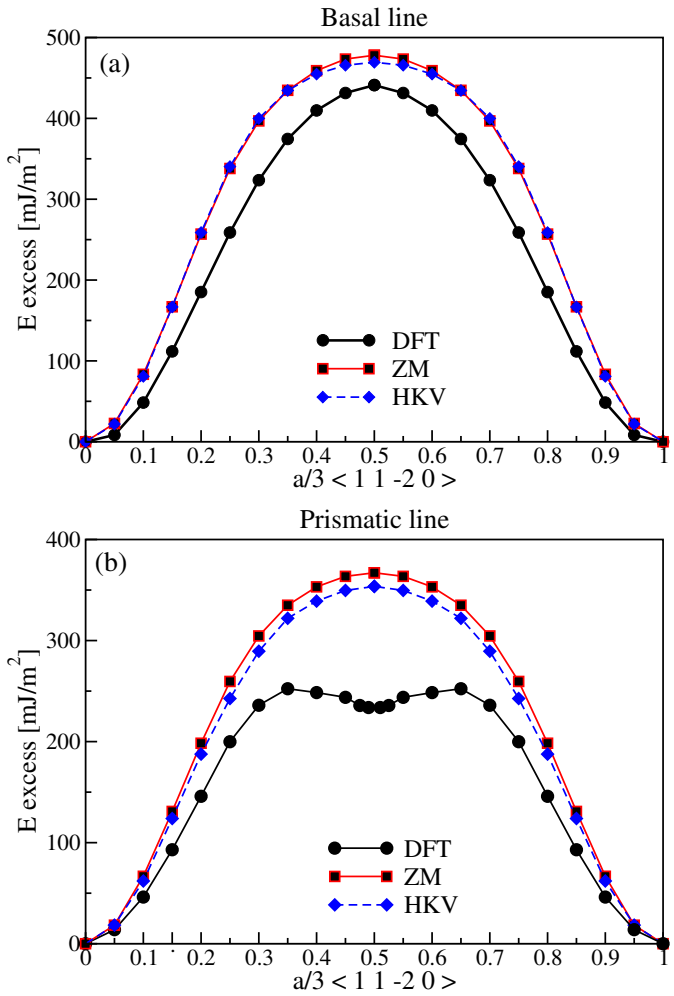

Figure 3. Hcp Ti basal (a) and prismatic (b) γ-lines in the $\frac{1}{3}\langle 1\,1\,\bar{2}\,0\rangle$ Burgers vector direction; circles: DFT calculations; Squares and rhombus: ZM and HKV EAM potential calculations, respectively.

Better exchange and correlation functionals need to be developed for a better description of these properties and consequently of the dislocation properties. However, with the state-of-the-art DFT calculations, the description is certainly good enough to reach an acceptable description of dislocations.

Using the calculated stacking fault energies, one can evaluate the R ratio of Legrand [8] for the determination of the easy slip plane for the $\frac{a}{3}\langle 1\,1\,\bar{2}\,0\rangle$ screw dislocation (see the introduction and results in table 3). The DFT results give $R = 1.1$, a value slightly higher than 1, leading to a preferential prismatic spreading as experimentally observed, and in agreement with our previous DFT calculations of the $\frac{a}{3}\langle 1\,1\,\bar{2}\,0\rangle$ dislocation core structure [16]. Our DFT R value is consistent with the one deduced from previously published DFT calculations [17, 18–33], which always lead to R values slightly larger than 1. The DFT ratio, just above 1, is much less than the one initially obtained by Legrand (2.5) in his TB calculations. His higher value was

mainly due to the underestimation of the prismatic $\gamma_{p,easy}$ stacking fault energy [8] by a factor of about 2. Unexpectedly, in their TB-BO calculations, Girshick and co-workers [13] found $R \approx 0.4$, a value much lower than 1, which is supposed to lead to a preferential basal spreading, whereas they observed a prismatic one. In that case, the difference comes essentially from an underestimation of the basal stacking fault energy by a factor of about 2 [13]. A similar underestimation of this basal stacking fault was also obtained by Béré [52]. It is surprising that these three TB calculations give so different values for the stacking fault energies, in particular for the basal one. In fact in the TB approach, to obtain the right energetic ordering of the hcp, fcc and bcc phases in compact close-packed structures, which conditions a good value for the basal stacking fault, one needs to make a calculation involving up to the sixth moment of the electronic density of states for the electronic energy calculation with the used recursion method. In Legrand's calculations, six moments were used, whereas in Girshick's and Béré's calculations, 9 and 32 moments were used, respectively. So, in these TB calculations the basal stacking fault excess energy, which originates mainly from the electronic part of the total energy[3] should be described with increasing accuracy with the number of used moments. As expected, the basal stacking fault energy is rather well evaluated by Legrand, but unexpectedly this evaluation is bad in Girshick's and Béré's calculations with very low values. In conclusion, increasing the accuracy in the description of the electronic band structure, instead of improving the description of the basal stacking fault, makes it dramatically worse. At odds with this, it seems to improve the description of the prismatic stacking fault excess energy. In that case, however, since the interatomic distances are quite modified, the excess energy is not solely due to the electronic energy.

Using the EAM results, we obtain an $R = 0.2$ value, leading to a preferential basal spreading, as we have observed in our EAM calculations of the $\frac{a}{3}\langle 1\,1\,\bar{2}\,0\rangle$ dislocation core structure [16]. The introduction of angular forces in the MEAM model is supposed to allow a better description of the basal stacking fault. In fact, the calculated MEAM [19, 33] basal γ_{I_2} excess energy is three times higher than the EAM one. However, it is still lower than the DFT one, leading to a R ratio significantly lower than 1 (0.4), since the prismatic fault energy is properly evaluated.

As previously discussed by Domain and Legris [18], the Legrand criterion is too simplified. In particular, it does not take into account the energy cost associated with the edge components of the dissociated basal dislocation. This extra energy cost means a preferential prismatic spreading even with R values lower than one. This explains the preferential prismatic spreading observed in the DFT calculations even with an R ratio only slightly larger than one, and similarly could explain the BO observed preferential spreading with $R = 0.4$. More puzzling is the large observed dispersion in the TB-based calculations of the basal stacking fault and its still poor description with the MEAM potential [19], since it may lead to erroneous dislocation calculations in these approaches. In fact with the MEAM potential, with an $R = 0.39$ ratio, if one considers the EAM results, which favor a basal spreading with R values around 0.25, and the BO potential, [13] which favors a prismatic spreading with $R = 0.3/0.4$, it seems that a prismatic spreading should be favored. Let us recall that, with the BO potential, the basal spreading is a metastable configuration only slightly more energetic than the prismatic one. From the results presented in [19], it is not clear whether a basal spreading exists or not and has a larger or lower excess energy than the prismatic one.

Let us now turn to the implications of the stacking fault energy values in terms of dislocation dissociation length and compare them with the previously published calculations of the core

[3] The interatomic distances and the coordination numbers are unchanged up to the second neighbor shell (included), which means an essentially unchanged repulsive energy in the model.

structure of the screw dislocation [16, 19]. The dissociation length d for a dislocation into partials $\vec{b}_2$ and $\vec{b}_3$ in the isotropic case is given by [5]

$$d = \frac{\mu}{2\pi\gamma}\left[(\vec{b}_2\cdot\vec{\xi}_2)(\vec{b}_3\cdot\vec{\xi}_3) + \frac{(\vec{b}_2\times\vec{\xi}_2)\cdot(\vec{b}_3\times\vec{\xi}_3)}{1-\nu}\right], \tag{2}$$

where γ is the stacking fault excess energy, μ and ν are the isotropic elastic constants and $\vec{\xi}_2$ and $\vec{\xi}_3$ are the two partial dislocation line directions. In this equation, the first and second terms represent, respectively, the contribution of the screw and edge parts of the partials. In our evaluations of d, we will take for μ the appropriate elastic shear constant (C_{66} for the prismatic dissociation and C_{44} for the basal one) and $\nu = (3B - 2C_{44}/2(3B + C_{44}))$, for the basal dissociation only. In fact, the second term in equation (2) disappears in the prismatic case since the partial dislocations are screw dislocations.

In the prismatic case, the obtained d_p values are 7.06 Å from the present DFT calculations and 5.54 Å (ZM) and 6.11 Å (HKV) from the EAM calculations. The DFT length is in agreement with the calculations of [19], which give a dissociation into partials separated by less than $2c = 9.3$ Å.

In the basal case, the dissociation lengths are estimated to be 3.49 Å in the DFT calculations and 15.18 Å (ZM) and 12.74 Å (HKV) in the EAM calculations. The very large differences between these dissociation lengths can be clearly attributed to the bad description of the basal stacking fault I_2 by the EAM interaction models. This result shows again that a very low basal stacking fault energy will favor the creation of partial dislocations stabilized by a large dissociation length and will consequently lead to a preferential basal spreading, as observed in the simulations carried out with the EAM potentials [16]. In the latter case, the dissociation length measured in the simulation of the screw $\frac{a}{3}\langle 1\,1\,\bar{2}\,0\rangle$ dislocation is in perfect agreement with the calculated one. In the DFT case, the very small value obtained for the basal dissociation length could explain why the basal core is not observed in the simulations [16].

It is interesting to compare the values of the dissociation lengths with those given by the MEAM potential [13] and by the TB BO potential [13], for which a prismatic spreading is found for the dislocation core. The prismatic dissociation lengths d_p could be estimated to be 4.55 Å in the MEAM case and 6.80 Å in the BO case (using the stacking fault energy for γ_{I_2} in equation (2)). In the basal case, the calculated values for d_b are 6.22 Å for the MEAM case and 8.31 Å for the BO one. The basal dissociation lengths obtained with these two models are larger than the present DFT ones but smaller than the EAM ones. Moreover, for these models, the fact that the basal dissociation lengths are of the same order as the prismatic ones implies that the two dislocation cores could exist. This is indeed the case for the BO model for which the two core structures were observed [13]. With the MEAM potential, only the prismatic core structure was presented in [19]; however, the basal spreading is very likely to exist. It is, nevertheless, difficult to predict which one of the two core structures would be found energetically stabler.

Using the Peierls–Nabarro model [62] for wide dislocations, we can also estimate the Peierls stress that would be needed for the gliding of the $\frac{a}{3}\langle 1\,1\,\bar{2}\,0\rangle$ screw dislocation in Ti. Only the gliding in the prismatic plane will be considered here since it is the one observed experimentally. It is given by [62]

$$\sigma_\mathrm{P}(\xi) = \frac{\mu b}{a'}\exp\left[-\frac{2\pi\xi}{a'}\right],$$

$$\xi = \frac{\mu b}{4\pi\tau_\mathrm{max}}.$$

In these formulae, μ is the elastic constant of interest, C_{66}, b is the Burgers vector, a' is the interplanar distance in the gliding direction, $c/2$, and τ_{max} is the maximum of the derivative of the prismatic γ-line (figure 3). This formulation follows from the assumption of a sinusoidal form for the restoring force. The estimation of the dislocation widths are found to be $\xi = 1.1b$ in the present DFT calculations, and $\xi = 1.0b$ and $\xi = 1.1b$ in the ZM and HKV EAM calculations, respectively, for a prismatic spreading. The Peierls stress can then be estimated to be ≈ 10 MPa using DFT, whereas it is close to 18 MPa with the ZM potential and to 8 MPa with the HKV potential. These values, although of the correct order of magnitude, are much lower than the experimental value measured in hcp Ti, which is around $\approx$100 MPa when extrapolated to 0 K [63]. This can be explained by the fact that the Peierls–Nabarro model is very simple, as it considers a dislocation spreading which is linear and a sinusoidal form for the restoring force. It is interesting to note that the Peierls stress obtained from the EAM potentials are not so different from the DFT one, although the prismatic stacking fault energy is very different. This is, in particular, due to the fact that the dissociation of the dislocation into partials is not considered in this simple model.

To conclude, from the present review, it is clear that only a very accurate description of both the γ-surfaces and the shear elastic constants is a pre-requisite for a correct description of the core structure and of the dynamics of dislocations in Ti. The available interaction models are, in this respect, not completely satisfactory. And even the TB-based models, which take into account the valence electronic degrees of freedom in an approximated way, are not satisfactory. The best model seems to be the MEAM model of Ghazisaeidi *et al* [19]. However, it has not been proven until now that the prismatic spreading is the stablest dislocation core configuration with this model. Even the DFT-pseudopotential calculations need to be improved through the development of more accurate exchange and correlation functionals, in particular to reach a better description of the shear elastic constants. Thus for now, only DFT approaches or a more precise TB approach, such as the DFT-based tight-binding approach (DFTB) should be able to properly describe the dislocation core structures in hcp Ti and consequently its plastic behavior. The development of such DFTB approaches or of improved MEAM models is essential in order to treat dynamical effects that are inaccessible to DFT calculations.

Acknowledgments

We would like to thank François Willaime and Chu Chun Fu for helping us get started with the SIESTA code. Our warm thanks go to Daniel Caillard and Alain Couret for very helpful discussions. This work has been supported by the ANR 'SIMDIM' contract no BLANC-0250. This work was also granted access to the HPC resources of CALMIP under the allocation 2011-p0685. Part of the calculations have been performed on the CINES computer center.

References

[1] Zope R R and Mishin Y 2003 Interatomic potentials for atomistic simulations of the ti-al system *Phys. Rev.* B **68** 024102

[2] Hammerschmidt T, Kersch A and Vogl P 2005 Embedded atom simulations of titanium systems with grain boundaries *Phys. Rev.* B **71** 205409

[3] Caillard D and J.-L. Martin 2003 *Thermally Activated Mechanisms in Crystal Plasticity* (Oxford: Pergamon)

[4] Yoo M, Morris J, Ho K and Agnew S 2002 Nonbasal deformation modes of hcp metals and alloys: role of dislocation source and mobility *Metall. Mater. Trans.* A **33** (3, Sp. Iss. SI) 813–22

[5] Hirth J P and Lothe J 1982 *Theory of dislocations* 2nd edn (Malabar, FL: Krieger)

[6] Bacon D and Vitek V 2002 Atomic-scale modeling of dislocations and related properties in the hexagonal-close-packed metals *Metall. Mater. Trans.* A **33** 721–33

[7] Legrand B 1984 Influence de la structure électronique sur la facilité relative des glissements dans les métaux de structure hexagonale compacte *PhD Thesis* Université Pierre et Marie Curie, Paris, France
[8] Legrand B 1985 Structure du coeur des dislocations vis 1/3a⟨1 1 $\bar{2}$ 0⟩ dans le titane *Phil. Mag.* A **52** 83–97
[9] Legrand P B 1984 Relations entre la structure lectronique et la facilit de glissement dans les mtaux hexagonaux compacts *Phil. Mag.* B **49** 171–84
[10] Legrand B 1986 Comment on 'computer simulation of dislocation cores in h.c.p. metals' by D J Bacon and M H Liang *Phil. Mag.* A **54** 43–4
[11] Liang M H and Bacon D J 1986 Computer simulation of dislocation cores in h.c.p. metals; II. Core structure in unstressed crystals *Phil. Mag.* A **53** 181–204
[12] Vitek V and Igarashi M 1991 Core structure of 1/3⟨1 1 $\bar{2}$ 0⟩ screw dislocations on basal and prismatic planes in h.c.p. metals: an atomistic study *Phil. Mag.* A **63** 1059–75
[13] Girshick A, Pettifor D G and Vitek V 1998 Atomistic simulation of titanium: II. Structure of 1/3 ⟨$\bar{1}$ 2 $\bar{1}$ 0⟩ screw dislocations and slip systems in titanium *Phil. Mag.* A **77** 999–1012
[14] Girshick A, Bratkovsky A M, Pettifor D G and Vitek V 1998 Atomistic simulation of titanium: I. a bond-order potential *Phil. Mag.* A **77** 981–97
[15] Ackland G J 1992 Theoretical study of titanium surfaces and defects with a new many-body potential *Phil. Mag.* A **66** 917–32
[16] Tarrat N, Benoit M and Morillo J 2009 Core structure of screw dislocations in hcp Ti: an *ab initio* DFT study *Int. J. Mater. Res.* **3** 329–32
[17] Domain C 2002 Simulations atomiques ab-initio des effets de l'hydrogène et de l'iode dans le zirconium *PhD Thesis* Université des Sciences et Technologies de Lille
[18] Domain C and Legris A 2004 Investigation of glide properties in hexagonal titanium and zirconium: an *ab initio* atomic scale study *IUTAM Symp. on Mesoscopic Dynamics of Fracture Process and Materials Strength: Solid Mechanics and its Applications (Osaka)* vol 115 ed Y Shibutani and H Kitagawa (Berlin: Springer) pp 411–20
[19] Ghazisaeidi M and Trinkle D 2012 *Acta Mater.* **60** 1287–92
[20] Soler J M, Artacho E, Gale J D, García A, Junquera J, Ordejón P and Sánchez-Portal D 2002 *J. Phys.: Condens. Matter* **14** 2745
[21] Perdew J P, Burke K and Ernzerhof M 1996 Generalized gradient approximation made simple *Phys. Rev. Lett.* **77** 3865–8
[22] Troullier N and Martins J L 1991 Efficient pseudopotentials for plane-wave calculations *Phys. Rev.* B **43** 1993–2006
[23] Daw M S and Baskes M I 1983 Semiempirical, quantum mechanical calculation of hydrogen embrittlement in metals *Phys. Rev. Lett.* **50** 1285–8
[24] Oh D J and Johnson R A 1988 Simple embedded atom method model for fec and hcp metals *J. Mater. Res.* **3** 471–8
[25] Igarashi M, Khantha M and Vitek V 1991 *Phil. Mag.* B **63** 603–27
[26] Cleri F and Rosato V 1993 Tight-binding potentials for transition metals and alloys *Phys. Rev.* B **48** 22–33
[27] Dai Y, Li J H and Liu B X 2009 *J. Phys.: Condens. Matter* **21** 385402
[28] Pasianot R and Savino E J 1992 Embedded-atom-method interatomic potentials for hcp metals *Phys. Rev.* B **45** 12704–10
[29] Baskes M I and Johnson R A 1994 *Modelling Simul. Mater. Sci. Eng.* **2** 147
[30] Fernndez J, Monti A and Pasianot R 1996 *J. Nucl. Mater.* **229** 1–9
[31] Hu W, Zhang B, Huang B, Gao F and Bacon D J 2001 *J. Phys.: Condens. Matter* **13** 1193
[32] Kim S P, Chung Y C, S.-C. Lee, Lee K R and Kim D S 2006 Co/coal/Co trilayer fabrication using spontaneous intermixing of Co and Al: molecular dynamics simulation *Mater. Sci. Eng.* B **135** 25–9
[33] Hennig R G, Lenosky T J, Trinkle D R, Rudin S P and Wilkins J W 2008 *Phys. Rev.* B **78** 054121
[34] Mehl M J and Papaconstantopoulos D A 1996 *Phys. Rev.* B **54** 4519–30
[35] Mehl M J and Papaconstantopoulos D A 2002 Tight-binding study of high-pressure phase transitions in titanium: alpha to omega and beyond *Europhys. Lett.* **60** 248
[36] Trinkle D R, Jones M D, Hennig R G, Rudin S P, Albers R C and Wilkins J W 2006 Empirical tight-binding model for titanium phase transformations, *Phys. Rev.* B **73** 094123
[37] Domain C 2006 *J. Nucl. Mater.* **351** 1–19
[38] Bercegeay C and Bernard S 2005 First-principles equations of state and elastic properties of seven metals *Phys. Rev.* B **72** 214101
[39] Vrit G 2007 Structure, stabilit et mobilit des dfauts ponctuels dans le zirconium hexagonal compact: tude *ab initio PhD Thesis* Universit Pierre et Marie Curie, Paris

[40] Wu X, Wang R and Wang S 2010 Generalized-stacking-fault energy and surface properties for hcp metals: a first-principles study *Appl. Surf. Sci.* **256** 3409–12
[41] Ostanin S A and Trubitsin V Y 1997 A simple model for calculating the P-T phase diagram of Ti *J. Phys.: Condens. Matter* **9** L491
[42] Jomard G, Magaud L and Pasturel A 1998 Full-potential calculations using the generalized-gradient corrections: structural properties of Ti, Zr and Hf under compression *Phil. Mag.* B **77** 67–74
[43] Kutepov A L and Kutepova S G 2003 Crystal structures of Ti under high pressure: theory *Phys. Rev.* B **67** 132102
[44] Barret C S and Massalski T B 1980 *Structure of Metals* 3rd edn (Oxford: Pergamon)
[45] Fisher E S and Renken C J 1964 Single-crystal elastic moduli and the hcp → bcc transformation in Ti, Zr and Hf *Phys. Rev.* **135** A482–94
[46] Simmons G and Wang H 1978 *Single Crystal Elastic Constants and Calculated Aggregate Properties: A Handbook* (Cambridge, MA: MIT Press)
[47] Wern H 2004 *Single Crystal Elastic Constants and Calculated Bulk Properties: a Handbook* (Berlin: Logos)
[48] Yip S 2005 *Handbook of Materials Modeling* B (Berlin: Springer)
[49] Domain C, Besson R and Legris A 2004 Atomic-scale *ab initio* study of the ZrH system: II. Interaction of H with plane defects and mechanical properties *Acta Mater.* **52** 1495–502
[50] Benali A, Lacaze C-Dufaure and Morillo J 2011 Density functional study of copper segregation in aluminum *Surf. Sci.* **605** 341–50
[51] Pond R C and Bollmann W 1979 The symmetry and interfacial structure of bicrystals *Phil. Trans. R. Soc. Lond.* A **292** 449–72
[52] Bere A 1999 Etude des défauts étendus dans le zinc, le cadmium et le titane par une méthode de liaison forte *PhD Thesis* Université de Caen/Basse Normandie, France
[53] De Boer F R, Boom R, Mattens W C M, Miedema A R and Niessen A K 1989 *Cohesion in Metals: Transition Metal Alloys* vol 1 (Amsterdam: North-Holland)
[54] Tyson W and Miller W 1977 Surface free energies of solid metals: estimation from liquid surface tension measurements *Surf. Sci.* **62** 267–76
[55] Partridge P 1967 *Metall. Rev.* **118** 169
[56] de Crecy A, Bourret A, Naka S and Lasalmonie A 1983 High resolution determination of the core structure of $1/3\langle 1\,1\,\bar{2}\,2\rangle$ edge dislocation in titanium *Phil. Mag.* A **47** 245–54
[57] Jaklevic R C, Lambe J, Mikkor M and Vassell W C 1971 Observation of electron standing waves in a crystalline box *Phys. Rev. Lett.* **26** 88–92
[58] Jaklevic R C and Lambe J 1975 Experimental study of quantum size effects in thin metal films by electron tunneling *Phys. Rev.* B **12** 4146–60
[59] Schulte F 1976 A theory of thin metal films: electron density potentials and work function *Surf. Sci.* **55** 427–44
[60] Feibelman P J 1983 Static quantum-size effects in thin crystalline, simple-metal films *Phys. Rev.* B **27** 1991–6
[61] Batra I P, Ciraci S, Srivastava G P, Nelson J S and Fong C Y 1986 Dimensionality and size effects in simple metals *Phys. Rev.* B **34** 8246–57
[62] Joós B and Duesbery M S 1997 Peierls stress of dislocations: an analytic formula *Phys. Rev. Lett.* **78** 266–9
[63] Naka S, Lasalmonie A, Costa P and Kubin L P 1988 The low-temperature plastic deformation of alpha-titanium and the core structure of a-type screw dislocations *Phil. Mag.* A **57** 717–40